## CHAPTER 10 — REMOTE SENSING

# CHAPTER 10 — REMOTE SENSING

## 10.1 Meteorological satellites

Satellite imagery can give important clues as to the dynamical processes occurring, especially if they are complemented by the forecaster's ability to associate this imagery with conceptual models (7.1). The principles of remote sensing and much about the interpretation of satellite images are in **Bader et al., 1995, Chapter 1.**

**Cracknell & Hayes (1991)**
**Scorer & Verkaik (1989)**

## 10.2 Image interpretation

In examining imagery the following should be borne in mind:

(i) time and date — for temperature regimes and likelihood of, say, snow or ice cover which in turn will indicate physical processes likely to be occurring, e.g. fog formation, convection;

(ii) geography of the field of view — hence radiation fog is often seen filling valleys and leaving ridges clear, while sea fog and stratus often follow the coastline.

### *10.2.1 VIS imagery*

(a) When considering albedo in VIS images, bear in mind that:
  (i) thick cloud is more reflective than thin cloud;
  (ii) water cloud is more reflective than ice cloud;
  (iii) cloud composed of small droplets is more reflective than cloud of large droplets.
  These criteria can act against each other (e.g. a Cu congestus will have a higher albedo than a glaciated Cb of the same depth).

(b) St and fog can have high albedos; oceans have low values except in diffuse or concentrated sun glint. However, absolute values are not necessarily too important — contrast is more readily discerned **(Fig. 10.1)**.

(c) Textural detail is clearest at low solar elevation (e.g. smoothness, striations, cellular or fibrous structure).

(d) Shadows and highlights are most easily seen at low solar elevation; they can help to differentiate partially superimposed cloud details at different levels.

(e) Sun glint on the polar orbiting satellite images:
  (i) The strongest reflection will be in the vicinity of the specular point where direct sunlight is reflected back to satellite.
  (ii) Sun glint increases in brightness towards latitude of overhead sun, i.e. brighter towards the south and in summer in northern latitudes.
  (iii) Clouds have enhanced brightness around the specular point; regions of calm winds or sheltered water may show up dark in the middle of sun glint.
  (iv) Absolutely calm water will give a very bright, concentrated response in a north–south oriented line. Small wavelets will give a broader, less bright response **(Fig. 10.2)**.

### *10.2.2 IR imagery*

(i) The degree of whiteness can generally be taken to be a function of the degree of coldness and density/thickness of the underlying cloud (e.g. thin clouds will appear darker than thick layers having the same top level.

(ii) Cloud elements not completely filling pixels will be representative of a temperature between cloud top and the earth's surface and may be difficult to detect, e.g. fair-weather Cu, thin Ci.

(iii) IR image generally has less texture due to lack of shadow, highlight features and resolution.

(iv) The temperate latitude convention is for low temperatures to be displayed as white and high temperatures as black.

(v) At high latitudes over cold surfaces there is lower contrast between high and low clouds.

### *10.2.3 Using IR with VIS imagery*

**Fig. 10.3** represents a decision table relating different cloud and surface types to different VIS and IR radiances; imagery is compared in **Fig. 10.4**.

**Bader et al. (1995), Chapter 1**
**DNOM (1982)**

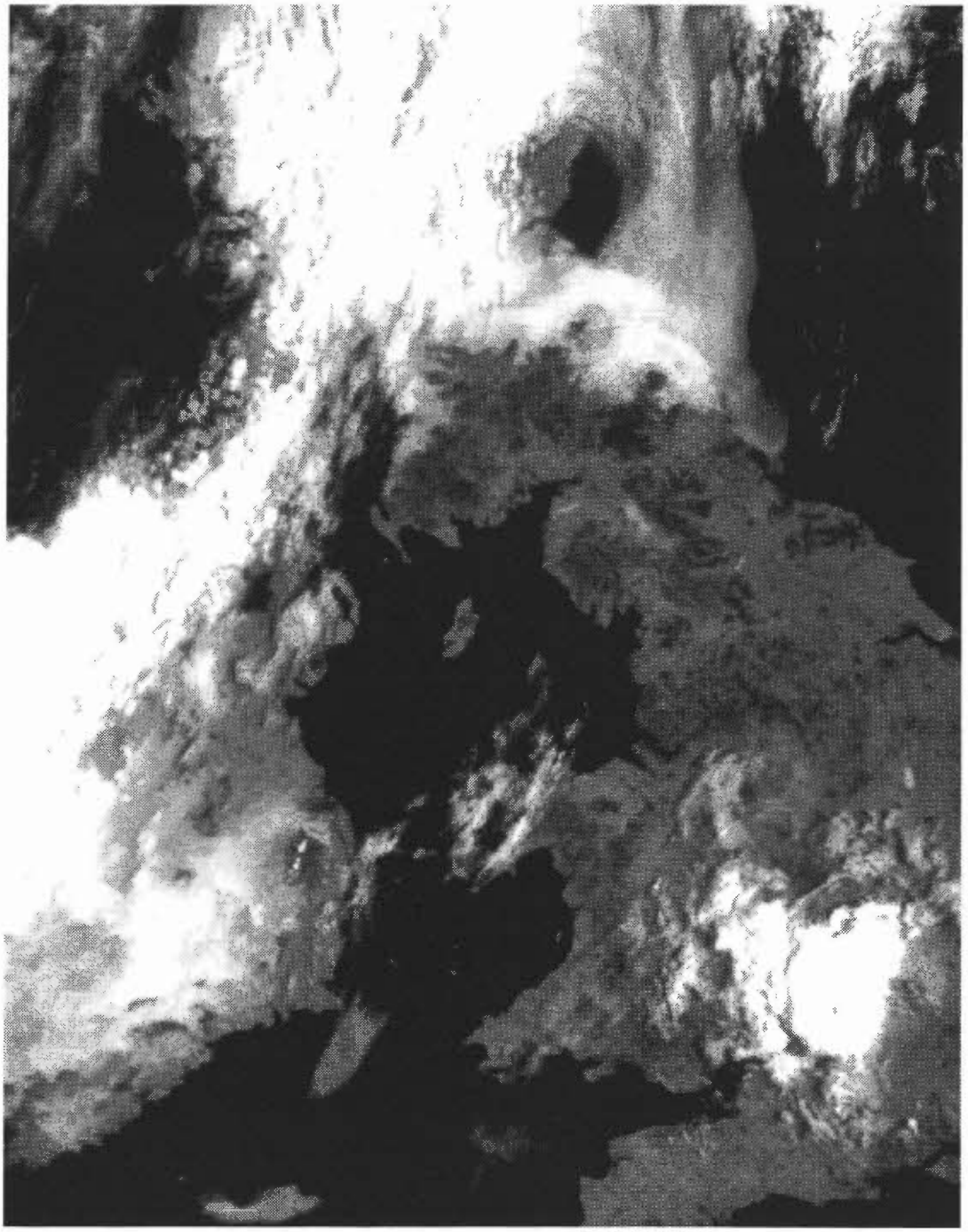

**Figure 10.1**. NOAA channel 2 (VIS) image at 0812 UTC on 24 May 1989. A large cumulonimbus anvil cloud over southern England shows up a small shadow cast by an overshooting top, probably extending into the stratosphere. A cold-frontal band extending from western Ireland to northern Scotland shows evidence of embedded convective activity. On the warm side of the front, sea fog is blown onto the coast of north-east England and south-east Scotland. This has rather straight, well defined edges over the sea, whereas inland its boundaries are determined by topography — the greatest inland penetration is between areas of high ground. The fog appears whiter over the land, where its albedo is little different from the much thicker clouds — this is because it is semi-transparent, and the sea is darker than the land. Much of central Ireland is also covered by fog, producing drizzle in places. The Wicklow Hills, just south of Dublin, are free of fog, and cumulus clouds have started to form due to insolation in the hilltops.

### *10.2.4 Water vapour imagery*

#### *10.2.4.1 Principles*

(i) WV imagery is usually displayed with the emitted radiation converted to temperature (as with IR imagery);

(ii) regions of high (low) tropospheric humidity appear cold (light)/warm (dark);

(iii) when the upper troposphere is dry, the radiation reaching the satellite originates from further down in the atmosphere, where it is warmer (darker image)

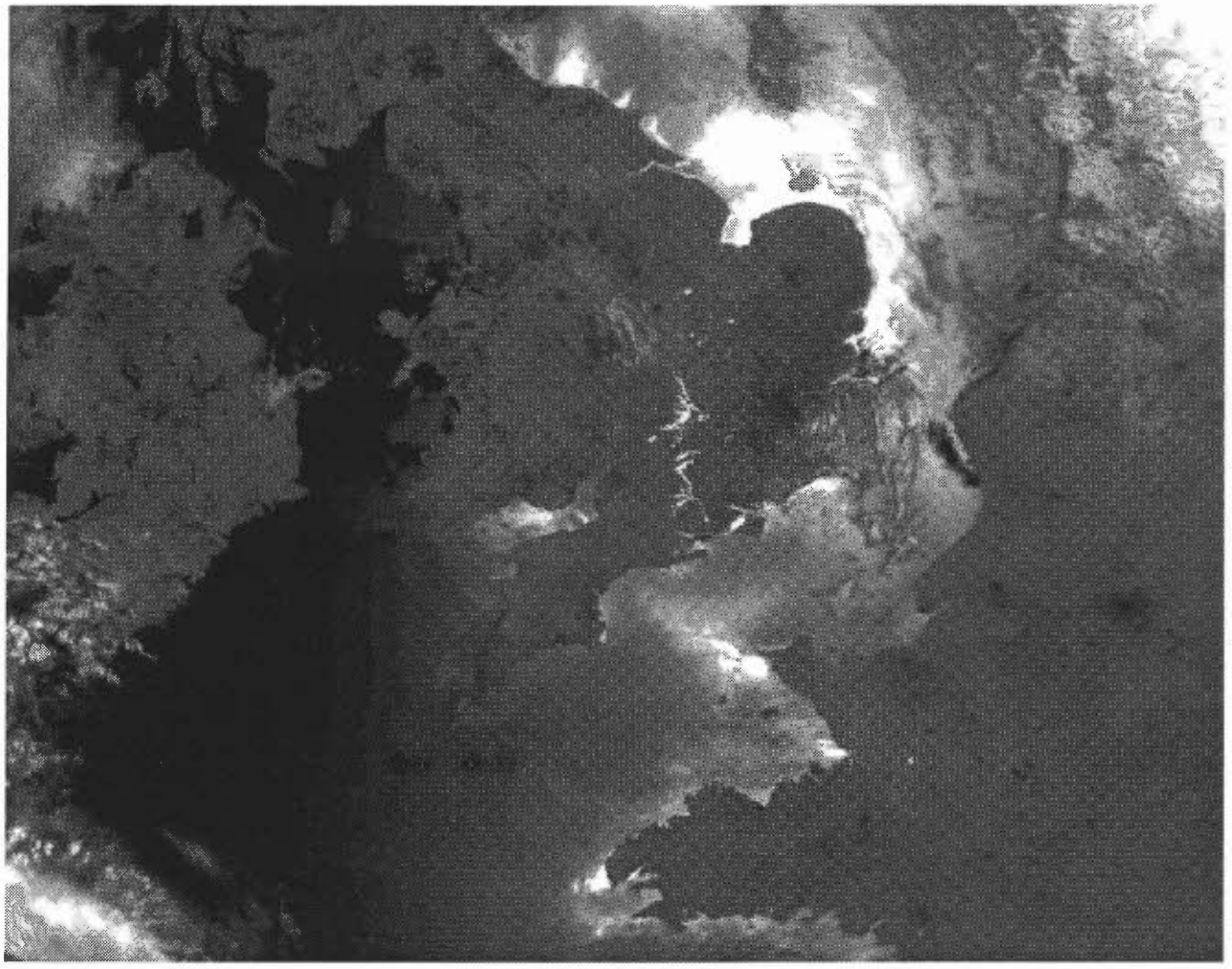

**Figure 10.2.** NOAA channel 2 (VIS) image at 0907 UTC on 19 July 1989. An anticyclone is centred over East Anglia. Sun glint reveals rivers and lakes in England despite their sub-pixel size. Differences in the intensity of sun glint result from variations in the smoothness of the sea. Sheltered waters near the coast show bright glint near the specular line, e.g. Brest peninsula, East Anglia, whilst slightly further from the specular line they appear dark, e.g in the Thames estuary and eastern Channel. Note that urban areas, e.g. Paris and London, as well as upland, have a lower albedo than other land surfaces.

#### *10.2.4.2 Interpretation*

(i) In a normally moist atmosphere, most of the WV radiation received by the satellite originates in the 300–600 hPa layer;
(ii) where the air is dry some radiation may come from layers as low as 800 hPa;
(iii) at higher latitudes the troposphere is colder with smaller temperature/height variations in lower latitudes, so that higher latitudes display a smaller range of grey shades;
(iv) the winter range of grey shades is less;
(v) moisture banding implies that brightness temperature may not be representative of air in lower layers — in particular, when WV imagery (dark) indicates a very dry upper troposphere (possibly low $\theta_w$/maximum vorticity) there may well be regions of high $\theta_w$ near the surface, leading to areas of deep convection;
(vi) moist air or cloud in the lower troposphere is not well depicted in WV imagery;
(vii) thick, high clouds such as Cb anvils, stand out prominently in both WV and IR.

**Bader et al. (1995), Chapter 1 DNOM (1982)**

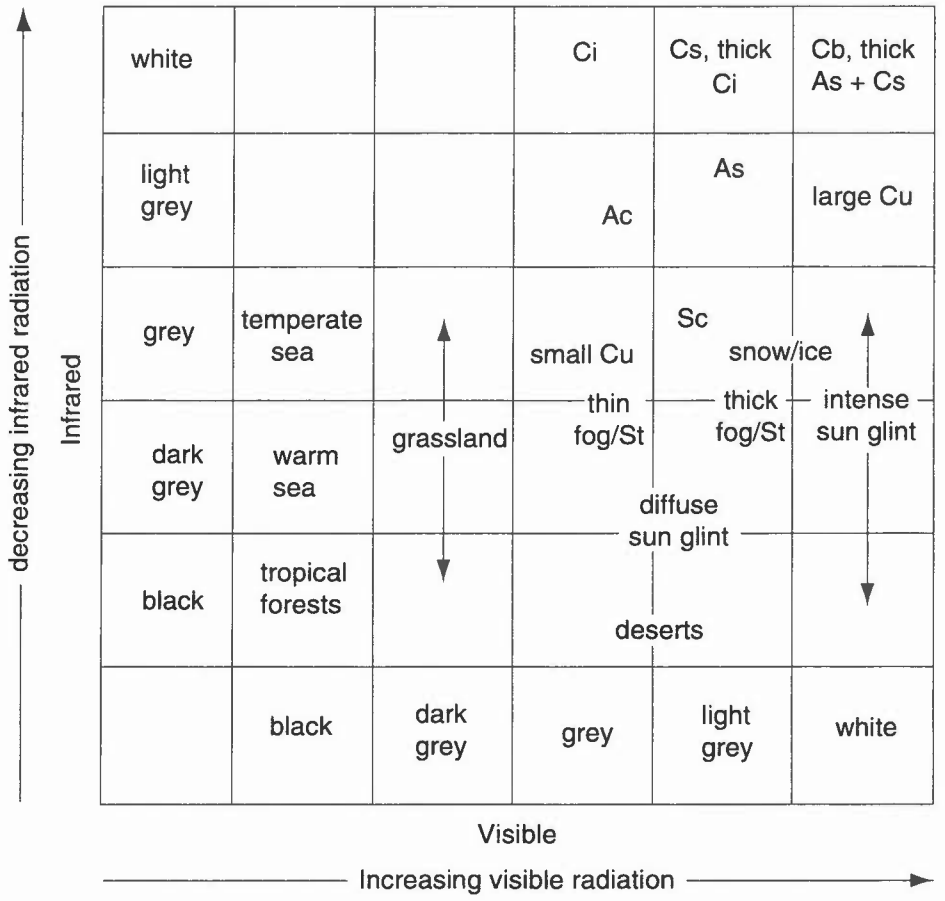


**Figure 10.3**. Decision table indicating typical radiances associated with clouds and different surfaces.

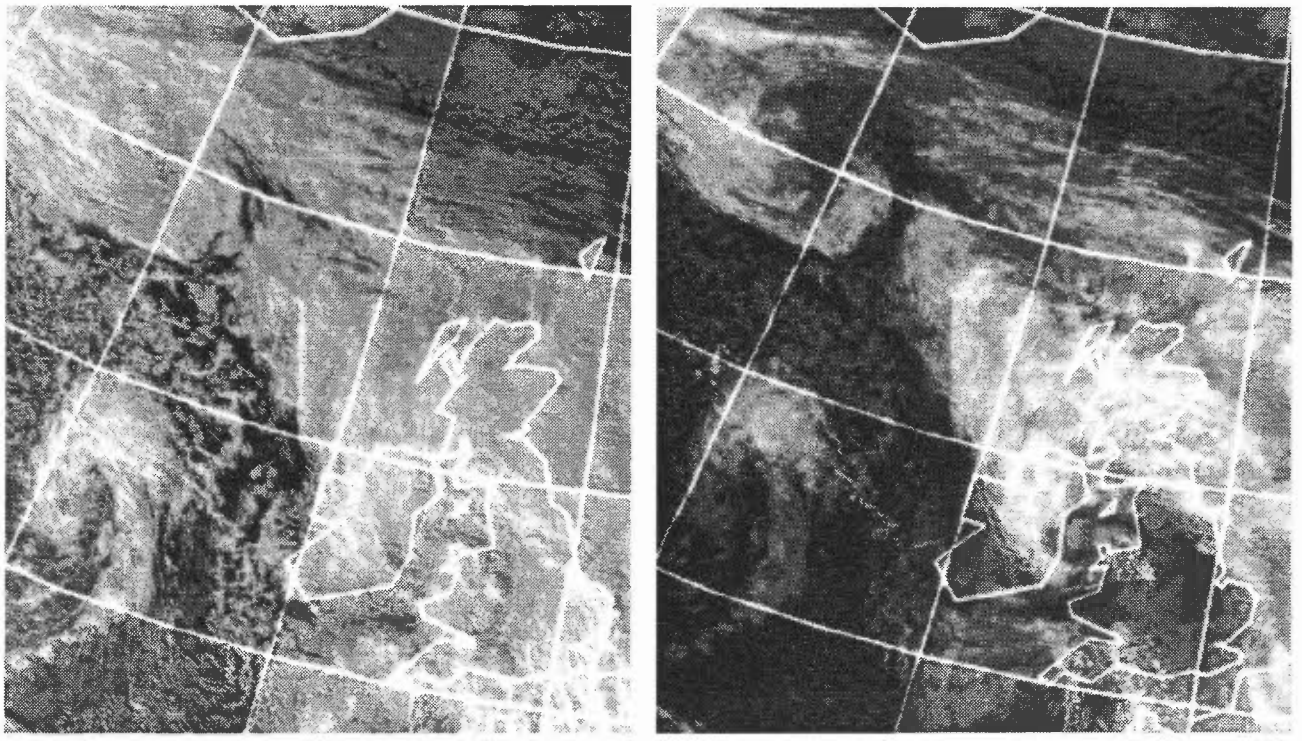

**Figure 10.4**. NOAA channel 2 (VIS) (left) and channel 4 (IR) (right), both at 1534 UTC on 22 October 1980. The IR image provides much detail which is not present in the VIS due to the lack of albedo contrast in the cloud features. The vortex structures to the south of Iceland and, in particular, in the Irish Sea are better represented in the IR image — these were both associated with surface depressions. The comma-shaped cloud appears to be a fairly active feature in the VIS image, whereas inspection of the IR image shows the comma tail to be of limited vertical development and therefore not likely to be associated with dynamical ascent.

## 10.3 Mesoscale interpretation — identification of cloud type and characteristics

### *10.3.1 Cumuliform*

(i) VIS imagery resolves small Cu better than IR.
(ii) IR imagery provides a better indicator of vertical development through grey-scale variations.
(iii) Dry-air advection may be indicated by warm brightness temperatures on water-vapour channels.
(iv) Cb appear very white in both VIS and IR with cloud aligned along the direction of any shear between cloud base and top; a clear edge will delineate cloud edge at the base and there will be a fuzzy edge where Ci plume spreads out (**Fig. 10.1**).
(v) Clusters of large Cb, growing in a sheared environment, produce extensive Ci shields which hide the lower cloud columns.
(iv) An arc-cloud (4.7.5) may be identifiable in imagery; it is associated with the region of surface outflow from cumulonimbus clouds and is a potential zone for daughter-cell Cb development (4.7.7.5).

**Bader et al. (1995), Chapter 6.4.3**
**Browning & Roberts (1995)**

#### *10.3.1.1 Cu patterns over land (see 4.6)*

(i) In light winds, preferred areas for cloud may be related to high ground, sun-facing slopes, or in association with troughs and sea-breeze convergence.
(ii) In more windy conditions (>10 kn) organized lines may appear; topographic forcing can lead to convergence giving streams of shower-producing clouds extending hundreds of kilometres downstream. Inland penetration of a sea breeze is illustrated in **Fig. 10.5** (see 1.3.1.1).
(iii) 'Cloud streets' appear as narrow lines of small Cu aligned along the low-level wind direction above the boundary layer; upper limit of cloud top is 10,000 ft, spacing is 2 to 8 km (some 3× the cloud depth) **(Fig. 10.6)**. There is often an inversion, with dry air above limiting the vertical development and preventing the spread into Sc by continual evaporation. Inland heating produces deeper convection which flattens out at the inversion (see 4.3.2.1).

**Monk (1987)**

#### *10.3.1.2 Cu patterns over sea*

Cloud streets occur, more widely spaced, downstream of land masses in fresh to strong cold off-shore airstreams; again orientation is a good indicator of low-level wind direction. Regular patterns of cells form, probably due to the homogeneous temperature distribution across the sea surface.

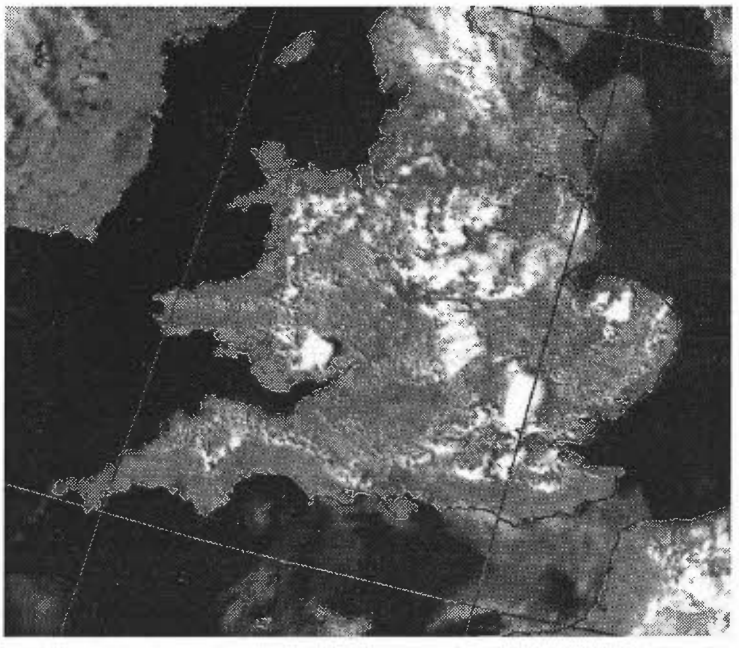

**Figure 10.5.** NOAA-7 AVHRR image at 1437 UTC on 7 July 1983. Inland penetration of the sea breeze around East Anglia and the south coast shown by the cloud-free margin.

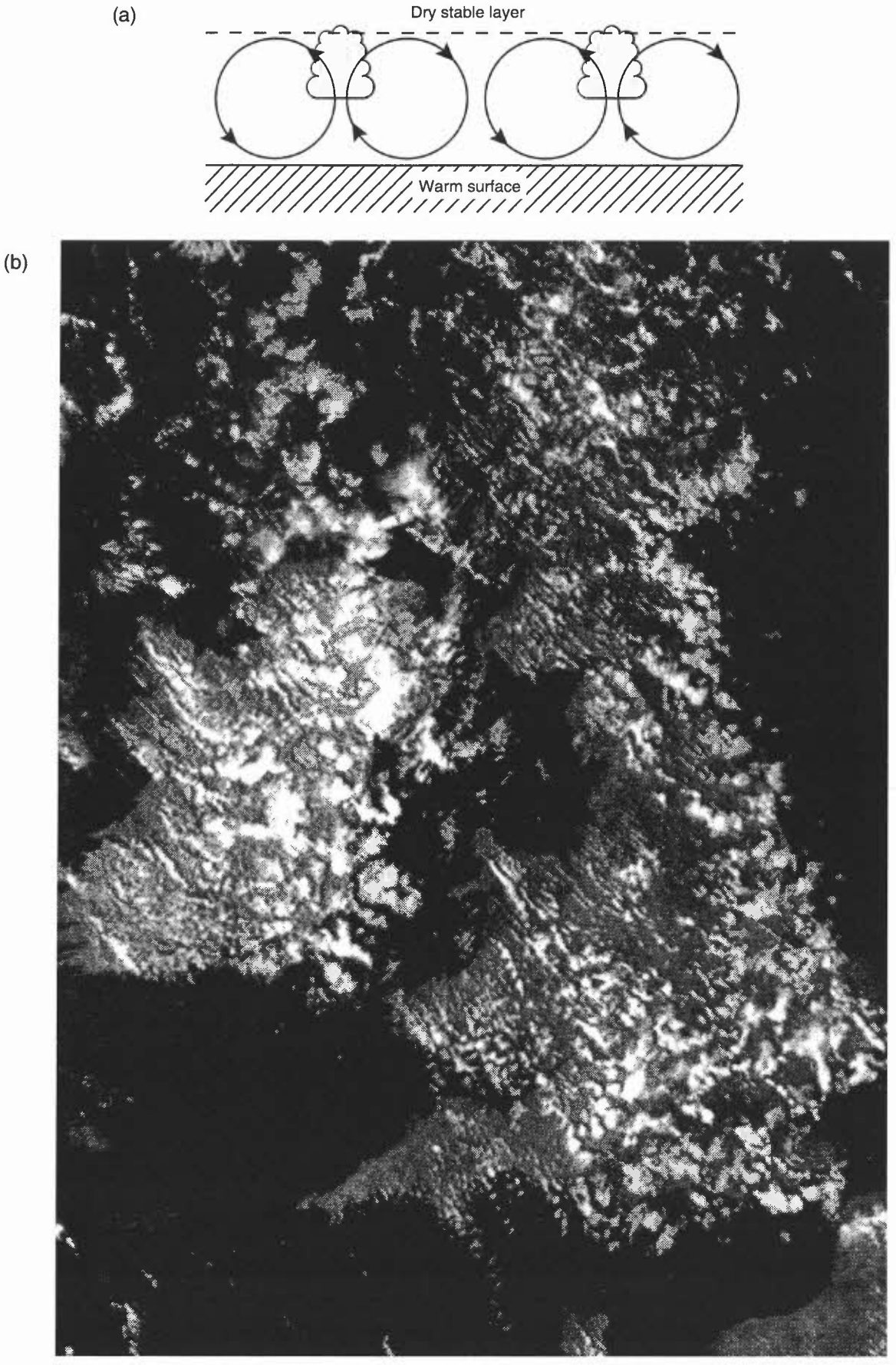


**Figure 10.6**. (a) Cross-section of circulations associated with cloud streets looking along the flow. Component of wind into the diagram leads to helical trajectories. (b) NOAA channel 2 (VIS) image at 1515 UTC on 16 April 1984 showing cumulus streets. It can be deduced that the low-level wind is from the WNW since the streets continue out over the southern North Sea.

*Open cells* **(Fig. 10.7)** characteristics:
(i) vigorous instability (through depths to 10,000 ft);
(ii) a large sea–air temperature difference;
(iii) usually cyclonic low-level flow and only small vertical wind shear;
(iv) aligned with the direction of thermal winds;
(v) open cell sizes often increase downwind with increasing instability over progressively warmer seas; however then anvils tend to obscure the polygons. The size of the cells is also related to the depth of convection (a ratio of 30:1 for cell diameter to depth of convection has been suggested).

*Closed cells* **(Fig. 10.7)** characteristics:
(i) an unstable layer is capped by a stable layer or inversion;
(ii) small differences in air–sea temperatures;
(iii) patterns are generally a feature of anticyclonic flow under a subsidence inversion and of areas of weak convection with low-level winds less than 20 knots.

**Browning et al. (1985)**

#### *10.3.1.3 Stratocumulus*

It is not unusual for Sc to display a closed cellular appearance when viewed under VIS; sensor resolution may not be good enough to resolve individual cells. In contrast IR images generally present a featureless sheet of grey which rarely displays the smoothness evident in fog or St.

### *10.3.2 Wave clouds, vortex sheets and lee eddies*

When conditions are right for *lee waves* (1.3.21), Sc can take on a wave pattern on passing over high ground **(Fig. 10.8)**. *Bow waves* can be triggered by isolated, steep-sided, mountainous islands for a wind speed greater than 30 kn **(Fig. 10.9).**

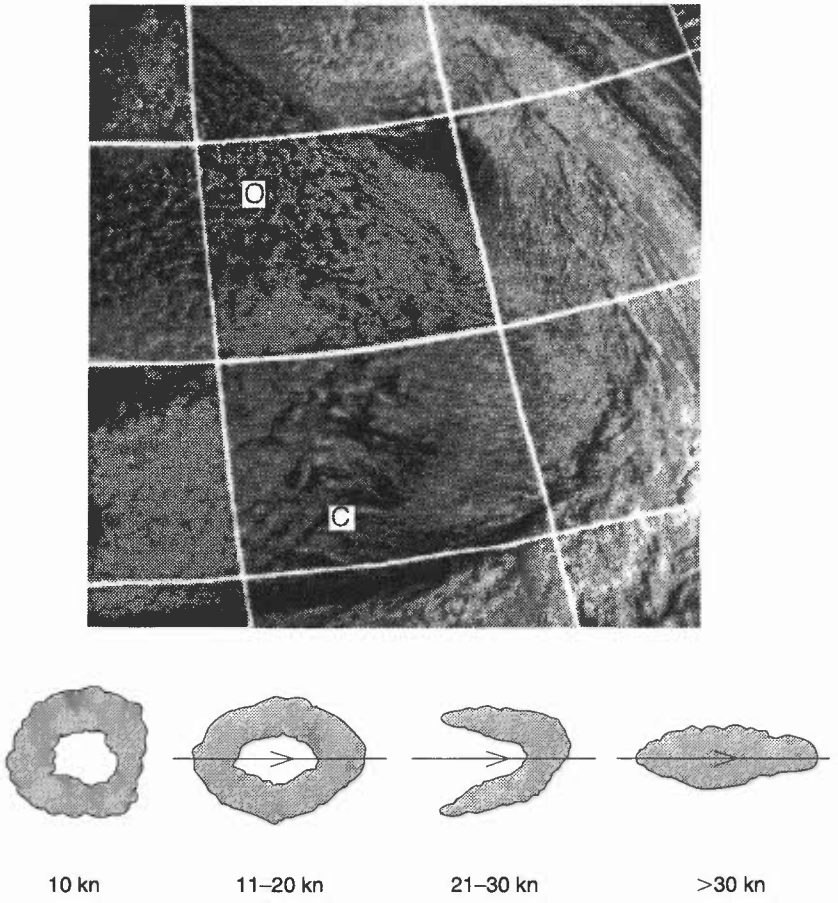


**Figure 10.7.** (top) NOAA channel 2 (VIS) image at 0927 UTC on 12 October 1980. Open (O) and closed (C) cell convection to the west of an Atlantic highlighted from the east by the morning sun. (bottom) Open cell shapes in different surface wind regimes.

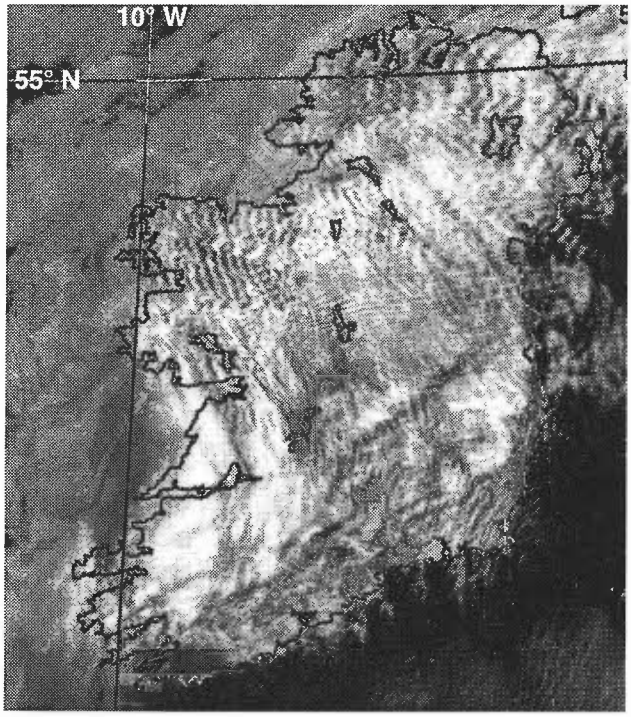


**Figure 10.8**. NOAA-11 VIS image at 1404 UTC on 20 May 1991 showing lee wave clouds over Ireland, and billow clouds.

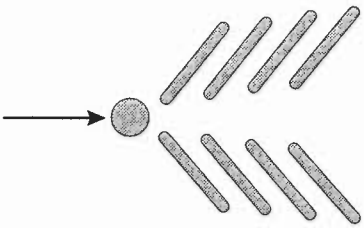

**Figure 10.9**. Bow waves forming downstream of an island.

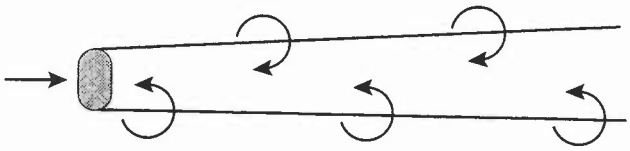

**Figure 10.10**. Vortex shedding from a steep-sided island.

Families of mesoscale *vortices* can be shed when there is:

(i) a strong inversion below obstacle height;
(ii) constant wind speed (10-30 kn) and direction with height.

The shedding generally appears with Sc cover; vortex shedding can sometimes be seen on the cold side of a frontal band downwind of Cape Farewell (southern tip of Greenland) **(Fig 10.10)** and frequently to the lee of the Canaries and Madeira, where they can extend for hundreds of kilometres downwind.

**Bader et al. (1995), Chapter 8**
**Scorer (1989)**

### *10.3.3 Stratus and fog*

(i) St/fog in a VIS image shows as a flat, uniformly textured surface and appears white or light grey. Boundaries are often sharply defined and coincide with topographical features **(Fig. 10.1)**.
(ii) In IR, St/fog appears as a uniformly grey field similar to Sc and is very difficult to identify, especially when thin.
(iii) St and Sc can be distinguished by the greater detail present in the VIS image. The lighter colour in IR imagery is associated with Sc.
(iv) Cloud over the sea having edges following the coastline (or with well defined edges far from land) is a sure sign of St/fog. However, with little depth, the St/fog may be hard to detect in IR since cloud-top temperatures and sea temperatures are similar.
(v) Vortex patterns similar to those associated with Sc are sometimes seen in St/fog fields.

*Fog* may be detected with the Advanced Very High Resolution Radiometer (AVHRR) by comparing brightness temperatures of the two channels 3 and 4 (providing there is no upper cloud):
(i) fog water drops have lower emissivity in Ch 3 (Ch 3<Ch 4);
(ii) land and sea surfaces have similar emissivity in Ch 3 and Ch 4 (Ch 3 = Ch 4);
(iii) thin, high cloud looks brighter in Ch 3 (Ch 3>Ch 4).

Thus at night white represents water cloud, grey — land or sea, and black — ice cloud.

### *10.3.4 Medium-level clouds*

(i) Altostratus produces a smooth, white response in a VIS image, mostly in association with frontal clouds when there is little to distinguish it from thick Cs. (It is often difficult to gauge the vertical extent of frontal cloud.)
(ii) The change from Ci to As is sometimes apparent at low solar elevation; at high elevation only the IR images will identify the individual cloud layers.
(iii) With no underlying cloud As appears light grey in VIS but cloud below will increase the whiteness of the image.
(iv) Ac is difficult to distinguish from As in VIS and IR since individual elements are too small to be resolved by sensors.
(v) Ac elements produced in the crests of lee waves will be clearly visible.
(vi) Convective elements associated with medium-cloud instability (Ac cast) appear similar to Cu clouds but produce brighter IR responses than are received from surface-based convection elements of similar size.

### *10.3.5 High-level clouds*

(i) Ci generally appears as mid- to light-grey in VIS imagery but thin Ci can be difficult to detect; IR response will be better. Increasing Ci thickness leads to a progressively whiter image.
(ii) In IR thin, patchy Ci may have a fibrous appearance and darker due to radiation from below.
(iii) Increasing Ci thickness leads to a progressively whiter VIS image, and Ci shields associated with frontal systems can be a brilliant white.
(iv) In IR, very thin, patchy Ci may have a fibrous, streaky appearance, but extensive formations tend to produce a continuous response, since IR radiation is effectively absorbed by ice.

#### *10.3.5.1 Contrails*

Contrails can have a sub-pixel response enough to be resolved; they are more likely to be resolved in IR imagery than VIS when the temperature difference with the background surface provides good contrast, although, in VIS, they sometimes cast noticeable shadows on lower cloud decks. Straight line appearance, sometimes criss-crossing, is unmistakable.

**Bader et al. (1995), Chapter 1**

### *10.3.6 Other features*

#### *10.3.6.1 Snow and ice cover*

Snow appears white to light grey in VIS depending on depth and freshness:
(i) reflectivity falls off rapidly as solar elevation to surface falls below 45°;
(ii) the older the snow the lower its reflectivity;
(iii) fresh snow at high solar elevation has an albedo of 85 to 90%; old snow 70% or less.

Underlying vegetation will influence the albedo:
(i) snow-covered forest has a lower albedo than snow-covered grassland, appearing mottled.
(ii) flat terrain appears smooth;
(iii) the 'dendritic' appearance of snow-free (or perhaps tree-filled) valleys in a mountainous terrain is unmistakable.

However, uniform snow fields are difficult to distinguish from cloud in VIS:
(i) they will have well defined edges and change only slowly with time;
(ii) clouds may by distinguished by shadows and change in detail between one image and another.

Off-shore winds, breaking up an ice field, will leave a characteristic dark band mapping the coastline.

#### *10.3.6.2 Ships' trails*

The seeding of clouds by particulates in ships' exhausts (principally in lower latitudes) can result in a narrow line of cloud sometimes extending for hundreds of kilometres. The trails, best seen in the VIS image, show up as an elongated bright region within the cloud, or as isolated streamers of cloud.

**Bader et al. (1995), Chapter 1**

#### *10.3.6.3 Dust clouds and smoke plumes*

Rising dust or sand may show as a blurring or brightening of the VIS image and also sometimes as an extensive cool area on IR, where VIS shows no cloud; they will show up well when blown over sea. Similarly smoke plumes from major fires and volcanoes can be detected in the VIS channel.

### 10.4 Image signatures of meso- and synoptic-scale processes

(i) Animated imagery from geostationary satellites is essential for identifying developments.
(ii) Overlaying appropriate model output with satellite imagery can reveal important phase or amplitude errors in the early stages of model runs (9.5).
(iii) Features of the imagery are useful in detecting model errors and giving advance warning of important developments, animated imagery being particularly useful.
(iii) Imagery, related to conceptual models (7.1), will help to identify significant cloud and the dynamical processes involved.

**McPherson et al. (1992)**

#### *10.4.1 Relationship between the jet axis, frontal location and cloud-band structure*

#### *10.4.1.1 Locating cold fronts*

(i) **Fig. 10.11** shows the positioning, relative to cold-frontal cloud bands, of the ana- and kata- cold front.
(ii) If 'rope' clouds are visible the cold front is best placed along them.
(iii) If not visible, then the ana-cold front is best placed ⅔ the way across the cloud band from the rear of the band and the kata-cold front towards the rear of the band.

#### *10.4.1.2 Locating warm fronts*

Although more difficult to position than cold fronts, the warm front is roughly 300 n mile from the leading edge of the frontal cirrus (**Fig. 10.12(a)**).

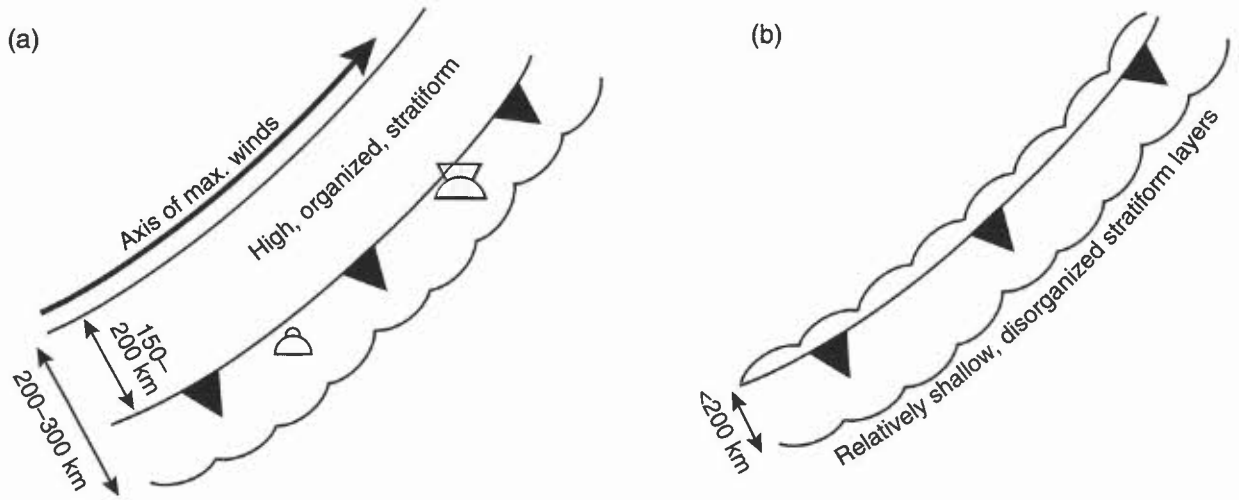


**Figure 10.11**. The cold front is best placed along 'rope' clouds, if visible. If these are not visible then the front is best placed, (a) ⅔ of the way across cloud band of an ana-cold front, and (b) towards the rear of cloud band of a kata-cold front.

### *10.4.1.3 Locating occlusions*

It is suggested that the occlusion is placed 50 to 100 km in from the rear edge of the frontal band (**Fig. 10.12(a)**).

### *10.4.1.4 Frontal cloud-band structure in relation to jet configuration*

**Fig 10.12** shows the nature of frontal cloud structure in relation to the configuration of the jet axis; the more active the front, the smaller the angle between the cold front and the jet (e.g. **Fig 10.12(b) & (c)**).

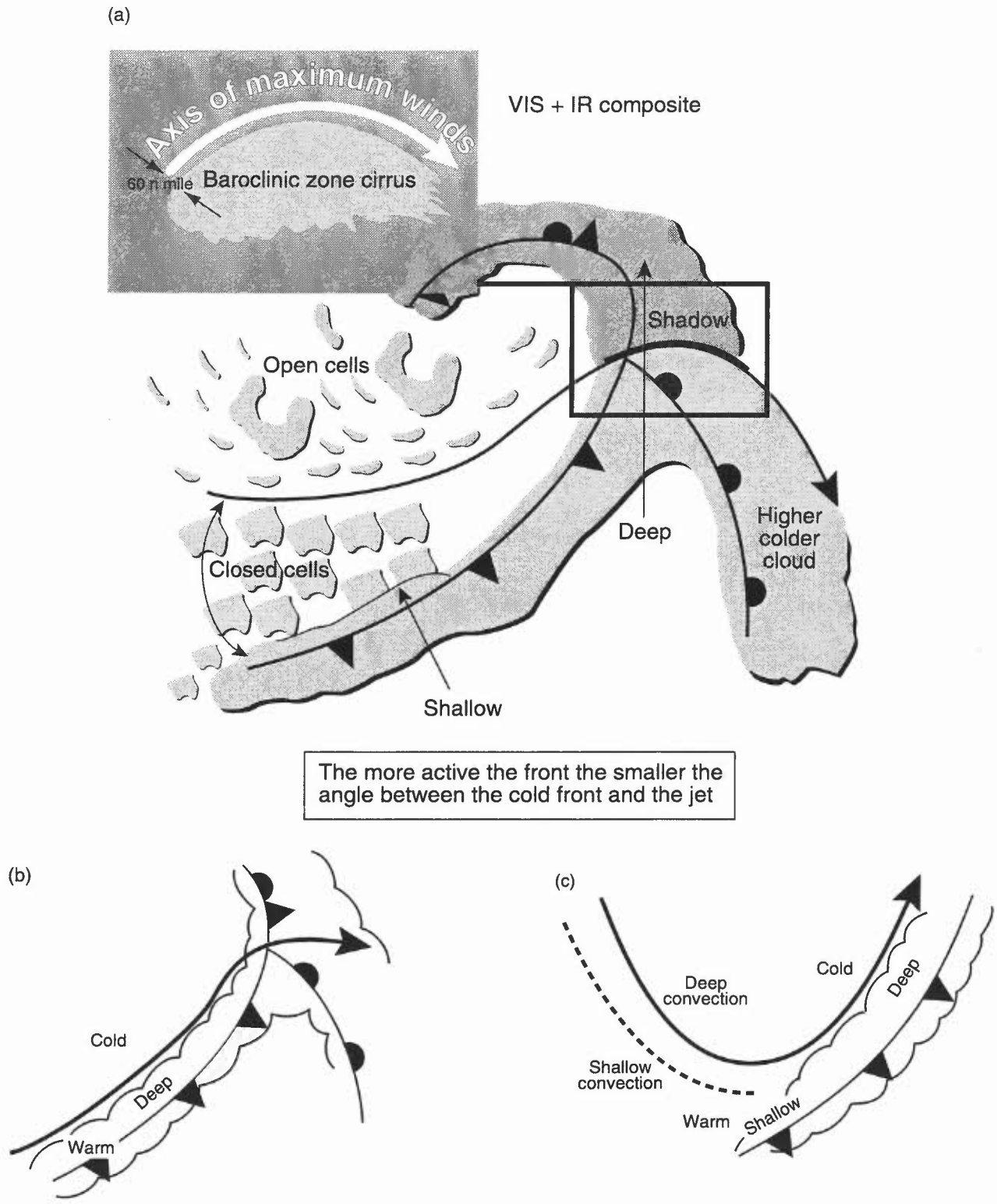


**Figure 10.12.** Satellite interpretation. (a) Positioning jet streams, (b) jet axis parallel to cloud band. Cloud vertically deep. Cloud edge aligned along jet axis but not necessarily in direction of jet winds. (c) Where jet is parallel to frontal band, cloud is deep and wide.

#### *10.4.1.5 Troughs and fronts over the ocean*

The upper trough may be difficult to position using satellite imagery. Here are clues as to its position:

(i) Where the trough intersects the front the cloud tops will often lower or fragment **(Fig. 10.13(a))**.

(ii) When the PVA ahead of the upper trough reaches 350 n mile upstream of a cold front, formation of a wave on the front can be expected **(Fig. 10.13(b))**.

(iii) Enhanced cumulus occurs in association with PVA ahead of an upper trough.

(iv) The relationship between comma-cloud formation, maximum vorticity areas and the diffluent thermal trough is shown in **Fig. 10.13(c)**. (Note: the comma shape is due to circulation within the relative airflow; vectorially adding the system translation velocity may give a trough relative to the earth's surface rather than a circulation.)

**Boyden (1963)**

### 10.5 Diagnosis of cyclogenesis

The 3-D detail required to forecast accurately the evolution of explosive cyclogenesis is very sensitive to initial conditions and not always correctly assimilated in the NWP initial conditions. There are characteristic image signatures which are not only associated with these intense storms, but more importantly from the forecasting point of view, precede the onset of winds of storm force 10 or more by as much as 24 hours (7.3.4).

#### *10.5.1 Image features*

#### *10.5.1.1 The baroclinic cloud leaf*

(i) Even if no cloud head is apparent the elongated 'S' shape of the cold side of the frontal cloud and the broadening of the band are characteristic of incipient cyclogenesis (the 'cloud leaf').

(ii) Only a small minority of cloud leaves develop into cloud heads.

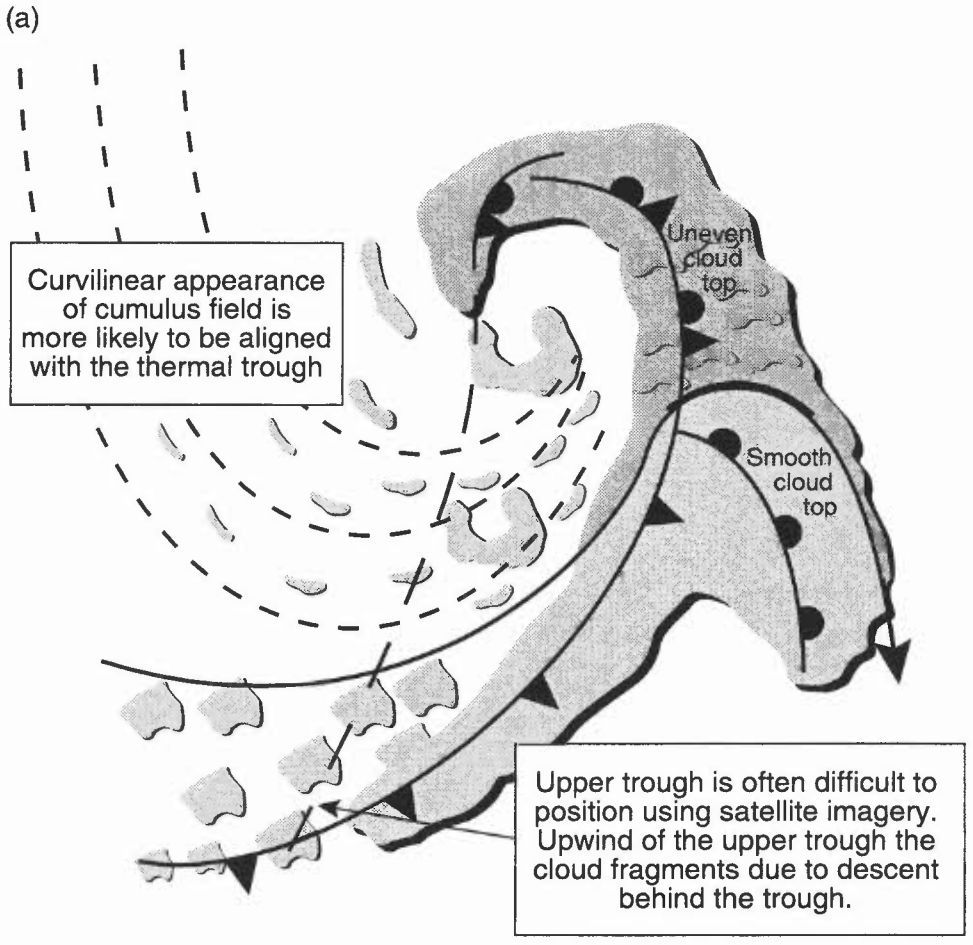


**Figure 10.13.** Satellite interpretation. (a) Troughs and fronts over the oceans, (b) upper troughs and frontal waves, and (c) troughs over the oceans — comma cloud.

(b)

The relationship between upper troughs and waves.

When the PVA ahead of the upper trough reaches 350 n mile upstream of a cold front, formation of a wave on the front can be expected.

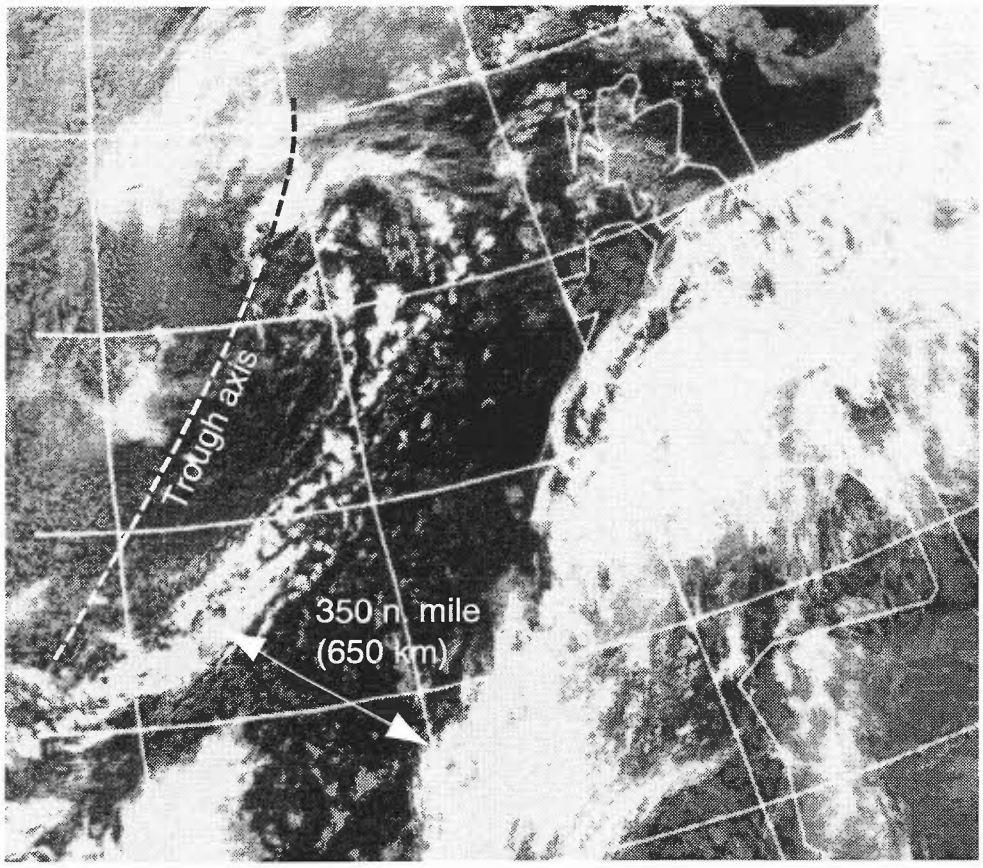


(c)

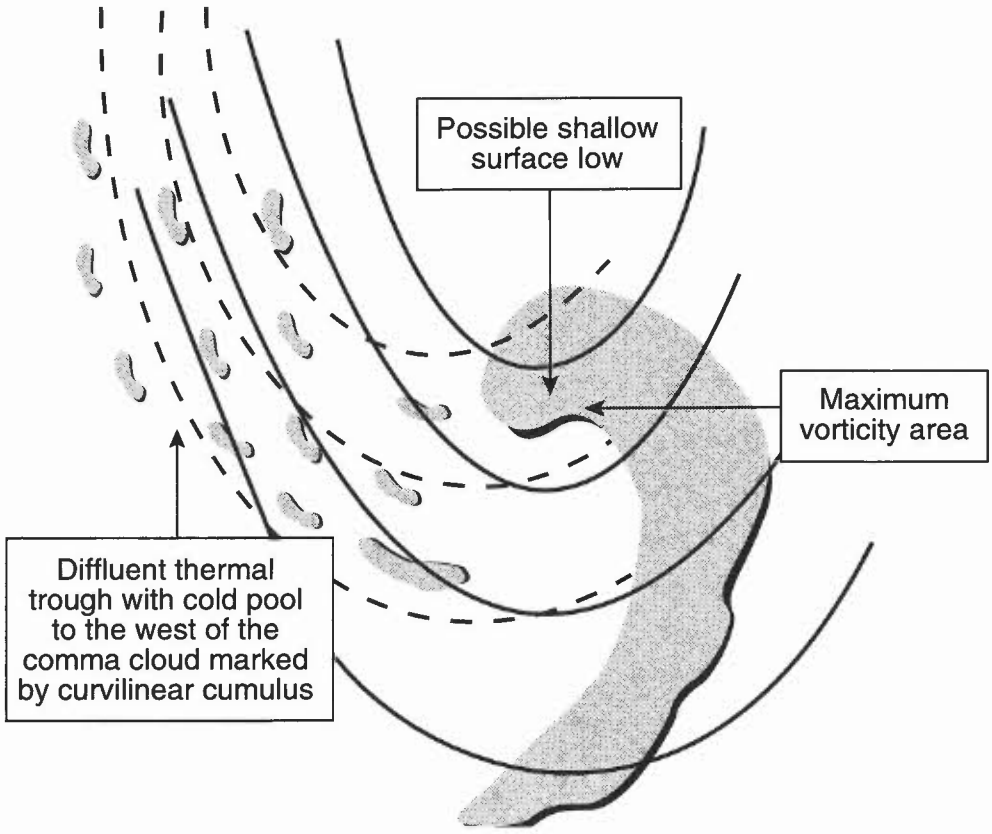


**Figure 10.13.** (Continued).

**Fig. 10.14** shows an IR image of a baroclinic cloud leaf associated with a depression (the surface front is unlikely to be significantly 'waved' in the early stages, despite the shape of the cloud structure (which is associated with upper flow and induced mid-tropospheric ascent)).

Estimating the position of the new low centre (**Fig. 10.15**):

(i) **Fig. 10.15** shows a schematic sequence of IR images at 6-hourly intervals of a vigorous cyclonic development over the north-eastern Atlantic.
(ii) Identify the point of inflection on the cold side of the the frontal boundary (P).
(iii) Draw a line perpendicular to the forward boundary of the cloud pattern.
(iv) The developing surface low (L) is likely to be along the warm side of the cloud boundary, about 2° latitude poleward of the intersection of the line with the cloud edge.
(v) With a PVA area close to the frontal zone, development is to be expected and the depression will take up a more central position underneath the cloud canopy (but still near the point of inflection).
(vi) If a dry slot forms, the surface low-pressure centre is likely to have migrated to a position under the cold boundary of the frontal band just behind the leading edge of the dry wedge.

**Weldon & Holmes (1991)**

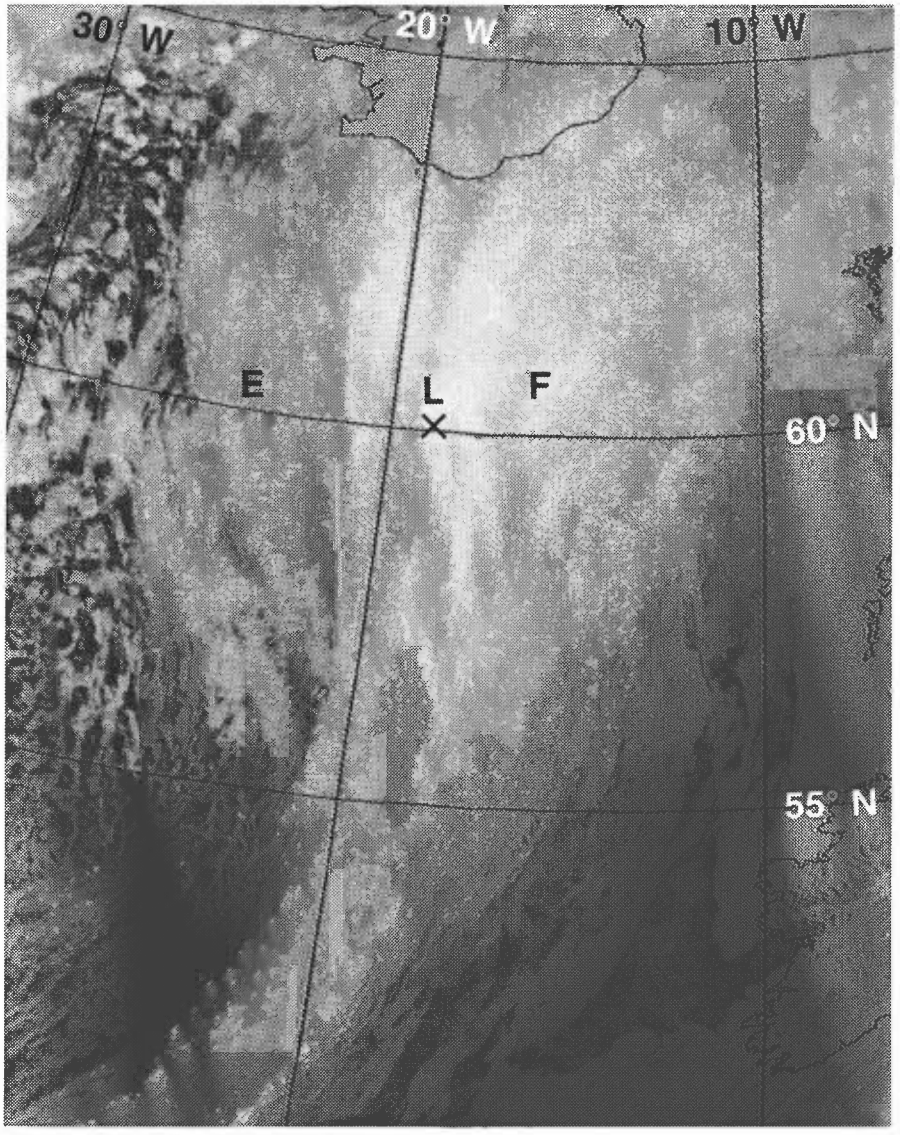


**Figure 10.14**. NOAA-11 IR image at 1336 UTC on 21 December 1988. Example of frontal cloud, F, and middle-level cloud, E (emergence of E is a sign of cyclogenesis). L is the developing surface low.

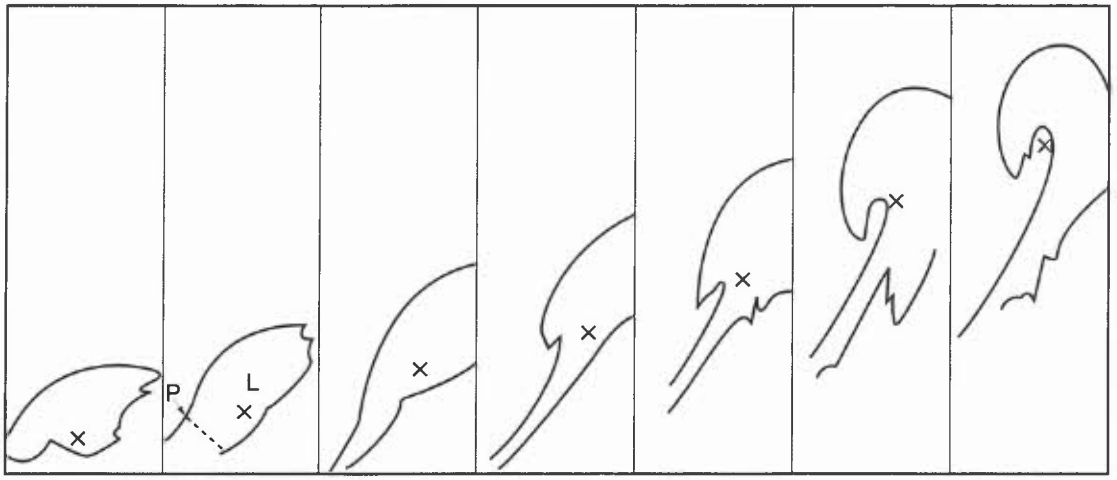


**Figure 10.15**. Sequence of schematic IR images associated with a developing depression. Images at 6-hourly intervals mark the surface depression. See 10.5.1.1 for explanation of construction on second image.

### *10.5.1.2 Development*

As cyclogenesis proceeds, a cloud E emerges from beneath the main frontal cloud F (**Fig. 10.16).** The shape of E and F will depend on the middle- and upper-tropospheric patterns (i.e. whether upper trough is confluent, diffluent, large or small amplitude). **Fig. 10.17(a)** shows seven types of cyclogenesis, **Fig. 10.17(b)** is the associated cyclogenesis decision tree; when E becomes particularly large and well-organized (a 'cloud head', see below), rapid deepening is more likely.

**Bader et. al (1995), Chapter 5.2**
**McLennan & Neil (1988)**
**Young (1993)**

### *10.5.1.3 The cloud head*

(i) Rapid cyclogenesis over the eastern Atlantic is invariably preceded by the cloud head, a cold-topped cloud structure extending polewards of, and separated from, the main frontal band (but elongated along a similar orientation, with a convex curved poleward edge); the cloud head is especially seen in confluent trough development.
(ii) The frontal development in **Fig. 10.18** has proceeded no further than the wave stage.
(iii) The head is indicative of rapid ascent, leading to the creation of low-level vorticity through vortex stretching and release of latent heat (7.3).

Note that in American terminology a cloud head is referred to as a 'comma' cloud and is not to be confused with the 'frontal comma cloud'.

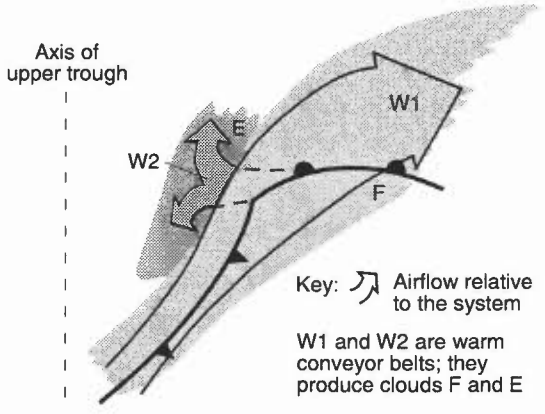


**Figure 10.16**. Emergence of cloud E is a sign that cyclogenesis is proceeding (after Bader et. al (1995), Chapter 5).

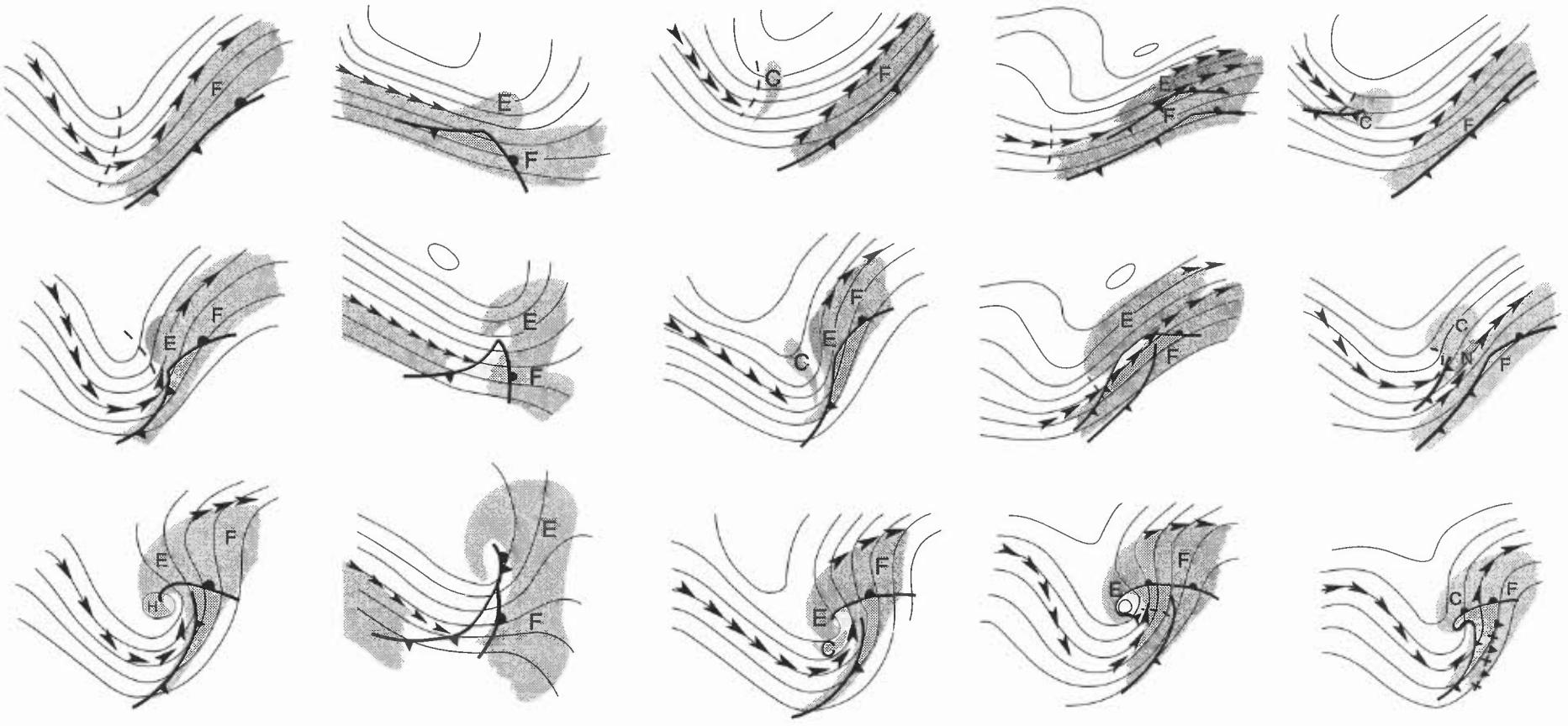


**Figure 10.17(a)**. The shape of clouds E and F associated with cyclogenesis will depend on middle- and upper-tropospheric patterns; seven types are illustrated (after Bader et. al (1995), Chapter 5). The diagrams aid your use of the decision tree (**Fig, 10.17(b)**).

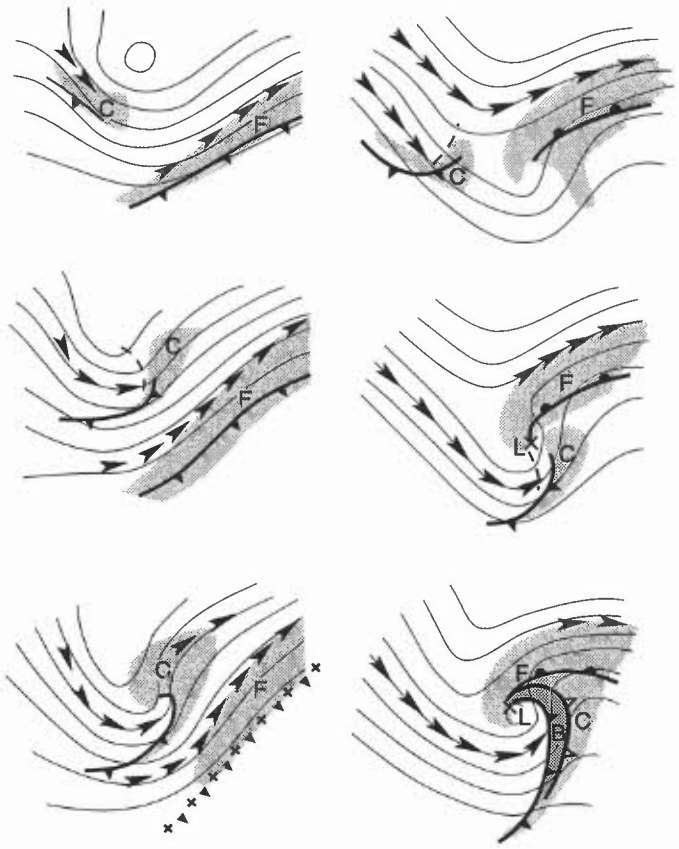


Cold air Split flow

**Figure 10.17(a).** (Continued).

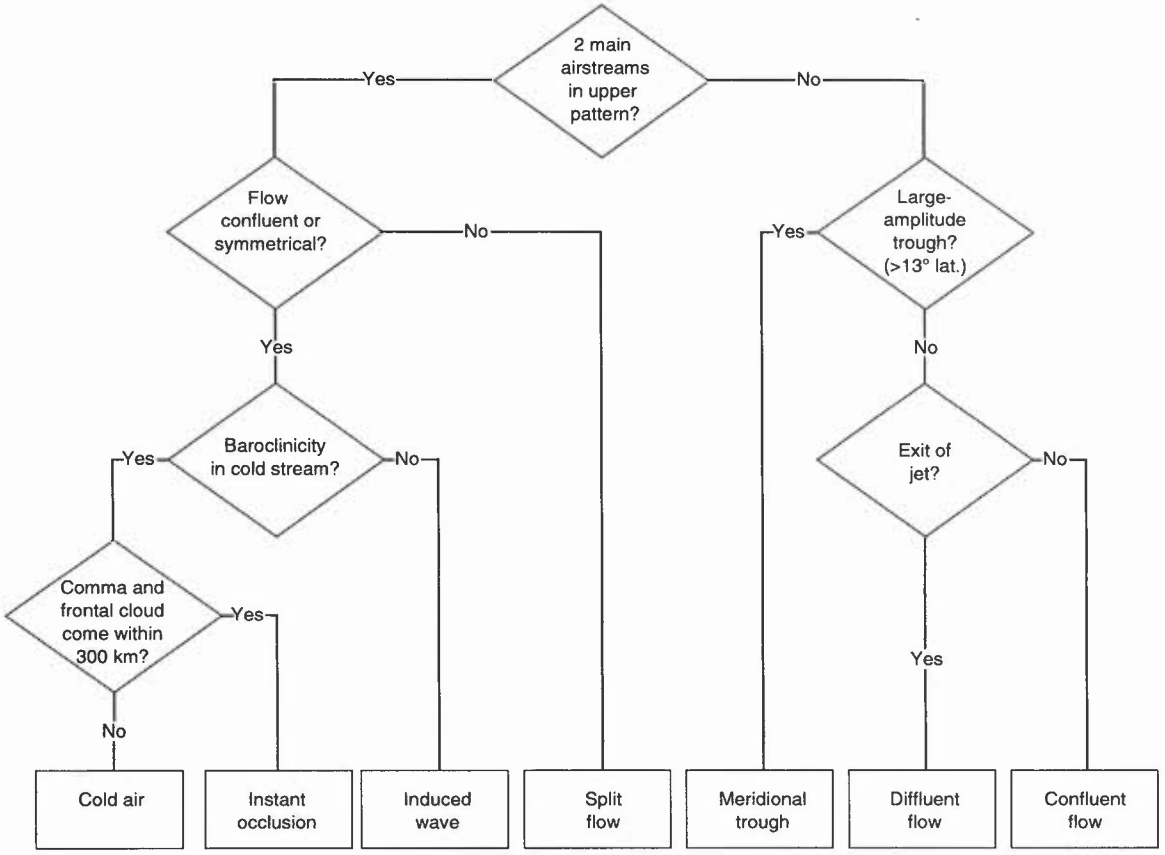


**Figure 10.17(b).** Decision tree for determining cyclogenesis type. A decision tree can be used to determine the appropriate archetype for cyclogenesis. It uses as input the characteristics of the cloud pattern and the upper flow. The path through the tree depends on whether the airflow around the upper trough is a single airstream (as in 'meridional trough') or has two separated streams (as in 'cold air').

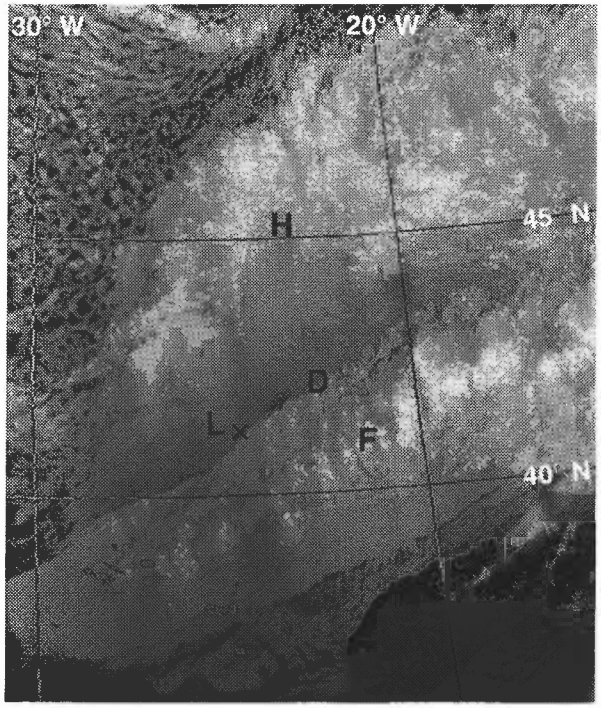


**Figure 10.18**. NOAA IR image for 0453 UTC on 15 October 1987. H marks the cloud head, D the dry slot and F the frontal cloud band.

#### *10.5.1.4 The dry wedge*

(i) Separating the cloud head (H) from the frontal band is a slot of relatively cloud-free air (dry slot or wedge), which forms upstream of the cloud head and becomes pronounced as it drives forwards (D in Fig 10.18).

(ii) The water vapour channel shows the dry wedge as a darkening feature, indicating stratospheric descent which accompanies upper tropospheric spin-up.

(iii) Clues to this dry air show up better in IR than VIS images since there is often warm-topped cloud with quite high albedo beneath the mid- to upper-tropospheric dry air.

(iv) Conducive to strong development also is the presence of deep convective cloud extending right up to and beneath the poleward edge of the cloud head; this indicates the close proximity of deep cold air and hence the strength of the baroclinicity.

**Bader et al. (1995), Chapter 5**
**Hewson (1993)**

### 10.6 Radar rainfall measurements

#### *10.6.1 Rainfall radar data limitations*

Although the display provides real-time information on the location of precipitation and associated frontal and convective development, the data have a number of limitations due to:

(a) spurious, non-meteorological echoes;

(b) radar rainfall not necessarily being that measured by a gauge at the surface;

(c) technical and meteorological causes (some of which are illustrated in **Fig. 10.19**), *particularly*:

(i) beam sampling at ever-increasing heights above the ground **(Fig. 10.20)** (important in cases of precipitation growth or evaporation below radar beam);

(ii) uncertainties in the radar reflectivity ($Z$)/rainfall-rate relationship (note that $Z$ is proportional to the 6th power of the drop radius, $R$). Real-time calibration against gauges reduces errors by identifying the radar-to-gauge data for distinct rainfall regimes.

However: the intensity of convective rain is often *overestimated* by a factor of 1.5,
the intensity of melting snow by up to a factor of 4.
Drizzle intensity is *underestimated* by a factor of up to 1.5.
Frontal rain and dry snow are usually well estimated;

(iii) from the 6th power relationship above it follows that drizzle and light rain are not detected even at short range;
(iv) orographic enhancement when pre-existing upper-level precipitation falls through very moist low-level air;
(v) detection at long range less likely with shallow precipitation and a low freezing level (this implies radar range performance is likely to be best in summer;
(vi) low-level evaporation, particularly ahead of warm fronts giving overestimate of surface rainfall and an error in the forecasting of beginning of precipitation;
(vii) large hail, causing serious overestimation;
(viii) an intense 'flare echo' may result due to multi-reflection of beam from hail and ground;
(ix) anomalous propagation — refraction of the radar beam can occur with a combination of a temperature inversion and, more important, a steep hydrolapse, for example, when there is a well-marked surface-based nocturnal cooling inversion. The most severe 'anaprop' occurs in anticyclonic conditions beneath a marked surface inversion; it rarely occurs when an inversion is more than 1200 m above the radar. Rain and anaprop can co-exist, especially when medium-level instability is present, in warm sectors, or when a cold front arrives following anticyclonic or ridge conditions (data from conventional observations must be monitored);
(x) signal attenuation on passing through rainfall (worse at shorter wavelengths, e.g. 3 cm compared with 10 cm) or behind hills (clutter may be mapped and electronically eliminated). Rainfall rates in cluttered areas can be estimated by interpolation. Higher beam elevation at close range can be used.
(xi) the 'bright band' due to beam intersecting the melting layer leading to overestimates in inferred surface rainfall;
(xii) radar sensitivity drift (perhaps over an hour or over many months).

In addition there can be interference from other radars, and a build-up of precipitation on the radome.

### *10.6.2 Meteorological features*

(i) Animation can show major changes in the horizontal wind field through convergence of rain cells or rotation of cells about a vortex centre.
(ii) The smallest rain areas are usually short-lived (1–2 hours); clusters of cells often persist longer.
(iii) Mesoscale rain areas, typically in bands, are frequently observed with lengths 50–500 km and persist for some time.
(iv) Large-scale rain areas have mesoscale features buried within them, typically one or two bands (often displaced from the surface front).
(v) These bands often travel faster than the organized rain area, with individual cells, in turn, moving faster than the band.
(vi) The cells within a band often have a major component of motion along the band. Mesoscale rainfall patterns thus reveal much about the fine-scale structure of the large-scale systems.
(vii) Showers are rarely totally random, but occur in organized convective areas that may persist well into the night (4.6).
(viii) A rain band can often be linked to a minor synoptic feature or to a line of convergence due to a sea-breeze front or to a topographical feature.
(ix) Extrapolation of well-defined entities can be effective to 6 hours ahead, some modification being allowed for development.
(x) Intense but rapidly moving cells may contribute little to point rainfall, but intense, slow moving cells or bands can give large accumulations.

The local forecaster should be aware of these limitations and features when monitoring rainfall areas and intensities; at the very least the display will be a valuable qualitative guide to precipitation distribution, to be used cautiously in conjunction with NWP and satellite data.

**Atlas (1990)**
**Bader et al. (1995), Chapter 2**
**Brown et al. (1991)**
**Collier (1989)**
**Conway & Browning (1988)**
**Kitchen et al. (1994)**

## 10.7 Sferics (see 4.7.4 — Lightning)

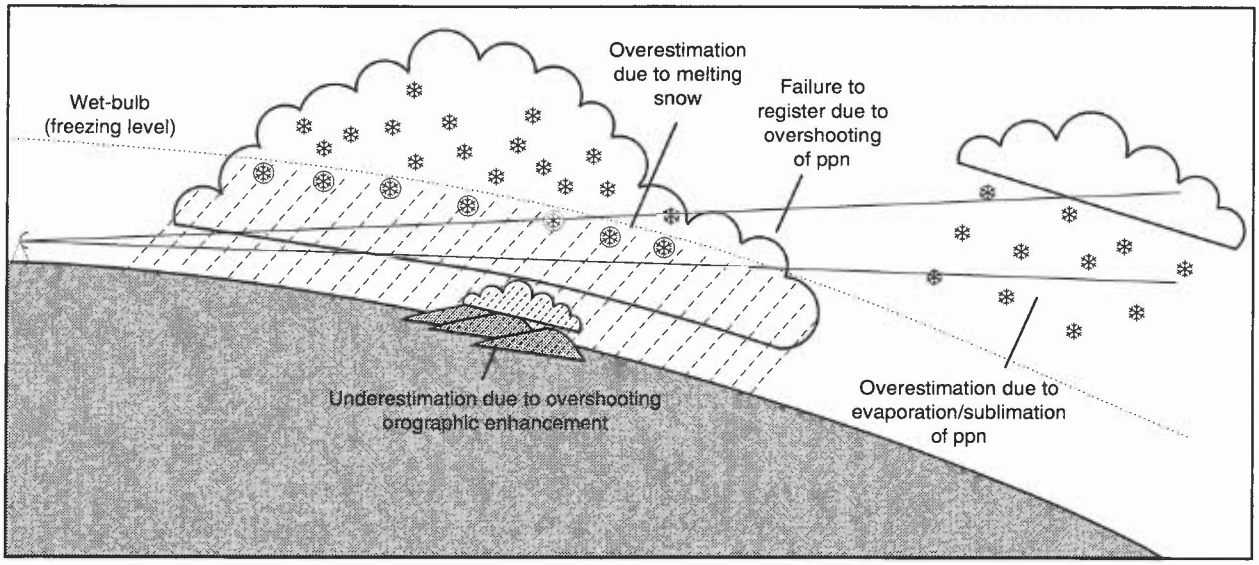


**Figure 10.19**. Some of the errors in surface precipitation rate estimates caused by sampling of precipitation away from the ground.

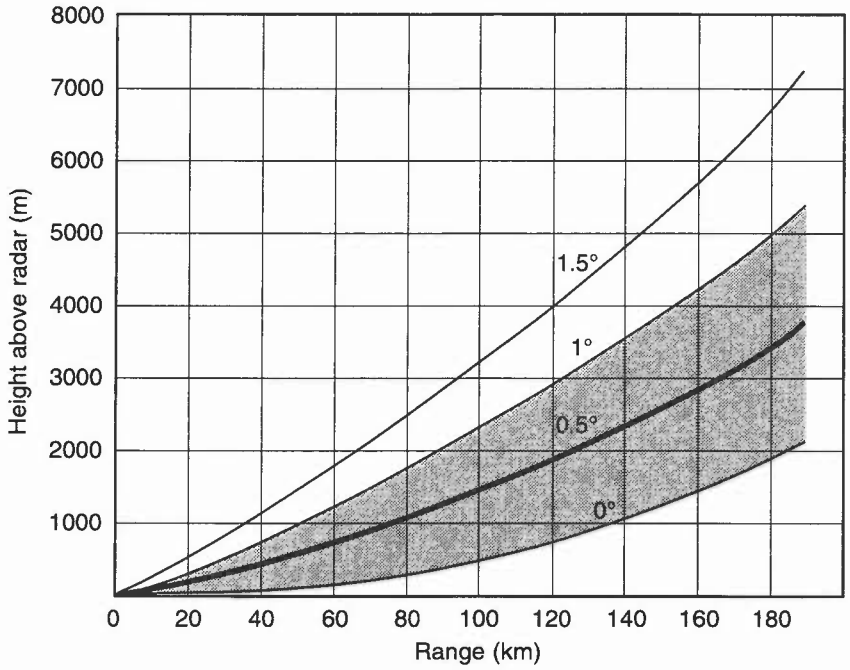


**Figure 10.20**. Height versus range for various beam elevations.

## BIBLIOGRAPHY

## CHAPTER 10 — REMOTE SENSING


Atlas, D, (Ed), 1990: Radar in meteorology. Proceedings of the Battan Memorial and 40th Anniversary Radar Meteorology Conference. Boston, American Meteorological Society.

Bader, M.J., Forbes, G.S., Grant, J.R., Lilley, R.B.E. and Waters, J., 1995: Images in weather forecasting. Cambridge University Press.

Boyden, C.J.,1963: Jet streams in relation to fronts and the flow at low levels. *Meteorol Mag*, **92**, 319–328.

Brown, R., Sargent, G.P. and Blackall, R.M., 1991: Hydrological applications of radar. pp. 219–228. Publisher: Ellis Horwood.

Browning, K.A. and Roberts, N.M., 1995: Use of satellite imagery to diagnose events leading to frontal thunderstorms: part 1 of a case study. *Meteorol Appl*, **1**, 303–310.

Browning, K.A., Eccleston, A.J. and Monk, G.A., 1985: The use of satellite and radar imagery to identify persistent shower bands downwind of the North Channel. *Meteorol Mag*, **114**, 325–331.

Collier, C.G., 1989: Applications of weather radar systems. Ellis Horwood.

Conway, B.J and Browning, K.A., 1988: Weather forecasting by interactive analysis of radar and satellite imagery. *Philos Trans R Soc Lond*on, **A324**, 299–315.

Cracknell, A.P. and Hayes, L.W.B., 1991: Introduction to remote sensing. Taylor and Francis.

DNOM, 1982: Weather satellite picture interpretation. Vols 1 and 2. DNOM memo 1/82. London, MoD, Directorate of Naval Oceanography and Meteorology.

Hewson, T.D. (Editor), 1993: The Fronts 92 Experiment: A Quicklook Atlas. Joint Centre for Mesoscale Meteorology, University of Reading, *Internal Report* No. 15.

Kitchen, M., Brown, R. and Davies, A.G., 1994: Real-time correction of weather data. *QJR Meteorol Soc*, **120**, 1231–1254.

McLennan, N. and Neil, L., 1988: Marine bombs program (phase II). Pacific Region tech. note 88-002.

McPherson, B., Wright, B.J. and Maycock, A.J., 1992: Formulation of the new Mesoscale Model data assimilation scheme. *Forecasting Research Paper* No. 143.

Monk, G.A., 1987: Topographically related convection over the British Isles. *Workshop on Satellite and Radar Imagery Interpretation,* pp. 305–324, Meteorological Office College.

Scorer, R.S. and Verkaik, A, 1989: Spacious skies. David and Charles.

Weldon, R.B. and Holmes, S.J., 1991: Water vapor imagery: interpretation and applications to weather analysis and forecasting. NOAA, Technical Report NESDIS 57.

Young, M.V., 1993: Cyclogenesis: interpretation of satellite and radar images for the forecaster. Bracknell, Meteorological Office, Forecasting Research Division Technical Report No. 73.